



Quantifying robustness of DFT predicted pathways and activity determining elementary steps for electrochemical reactions

Cite as: J. Chem. Phys. **150**, 041717 (2019); <https://doi.org/10.1063/1.5056167@jcp.2019.IFEC2019.issue-1>
Submitted: 12 September 2018 . Accepted: 14 November 2018 . Published Online: 19 December 2018

Dilip Krishnamurthy , Vaidish Sumaria, and Venkatasubramanian Viswanathan 

COLLECTIONS

Paper published as part of the special topic on [Collection](#) and [Interfacial Electrochemistry and Photo\(electro\)catalysis](#)



View Online



Export Citation



CrossMark

ARTICLES YOU MAY BE INTERESTED IN

[Quantifying robustness of DFT predicted pathways and activity determining elementary steps for electrochemical reactions](#)

The Journal of Chemical Physics **150**, 041717 (2019); <https://doi.org/10.1063/1.5056167>

[Uncertainty quantification of DFT-predicted finite temperature thermodynamic properties within the Debye model](#)

The Journal of Chemical Physics **151**, 244702 (2019); <https://doi.org/10.1063/1.5132332>

[A climbing image nudged elastic band method for finding saddle points and minimum energy paths](#)

The Journal of Chemical Physics **113**, 9901 (2000); <https://doi.org/10.1063/1.1329672>

Lock-in Amplifiers
up to 600 MHz



Quantifying robustness of DFT predicted pathways and activity determining elementary steps for electrochemical reactions

Cite as: J. Chem. Phys. 150, 041717 (2019); doi: 10.1063/1.5056167

Submitted: 12 September 2018 • Accepted: 14 November 2018 •

Published Online: 19 December 2018



View Online



Export Citation



CrossMark

Dilip Krishnamurthy,¹  Vaidish Sumaria,¹ and Venkatasubramanian Viswanathan^{1,2,a} 

AFFILIATIONS

¹Department of Mechanical Engineering, Carnegie Mellon University, Pittsburgh, Pennsylvania 15213, USA

²Department of Chemical Engineering, Carnegie Mellon University, Pittsburgh, Pennsylvania 15213, USA

^avenkvis@cmu.edu

ABSTRACT

Density functional theory calculations are being routinely used to screen for new catalysts. Typically, this involves invoking scaling relations leading to the Sabatier-type volcano relationship for the catalytic activity, where each leg represents a unique potential determining an elementary step. The success of such screening efforts relies heavily not only on the prediction robustness of the activity determining step, but also on the choice of the descriptor. This becomes even more important as these methods are being applied to determine selectivity between a variety of possible reaction products. In this work, we develop a framework to quantify the confidence in the classification problem of identifying the potential determining step for material candidates and subsequently the pathway selectivity toward different reaction products. We define a quantity termed as the classification efficiency, which is a quantitative metric to rank descriptors on the basis of robustness of predictions for identifying selectivity toward different reaction products and the limiting step for the corresponding pathway. We demonstrate this approach for the reactions of oxygen reduction and oxygen evolution, and identify that ΔG_{OOH^*} is the optimal descriptor to classify between $2e^-$ and $4e^-$ oxygen reduction. We further show that ΔG_{OH^*} and ΔG_{OOH^*} have comparable performance in identifying the limiting step for $4e^-$ oxygen reduction reaction. In the case of oxygen evolution, we study all possible 2 descriptor models and identify that $\{\Delta G_{\text{OOH}^*}, \Delta G_{\text{O}^*}\}$ and $\{\Delta G_{\text{OH}^*}, \Delta G_{\text{O}^*}\}$ both are highly efficient at classifying between $2e^-$ and $4e^-$ water oxidation. The presented methodology can directly be applied to other multi-electron electrochemical reactions such as CO_2 and N_2 reduction for improved mechanistic insights.

Published under license by AIP Publishing. <https://doi.org/10.1063/1.5056167>

I. INTRODUCTION

Density functional theory (DFT) calculations have been used extensively to understand reaction mechanisms and products for electrochemical reactions. The formulation of the computational hydrogen electrode has allowed the determination of free energy diagrams (FEDs), which have been used to extract the thermodynamic limiting potentials, and have been used quite successfully in rationalizing trends in reactivity over a broad range of materials for oxygen electrochemistry.¹⁻⁵ While there has been tremendous success in determining reactivity trends for a particular electrochemical reaction, there has been very limited success

in determining selectivity for electrochemical reactions, e.g., $2e^-$ vs. $4e^-$ oxygen reduction and evolution, and oxygen evolution vs. chlorine evolution.⁶⁻¹⁰ The electrochemical reactions of great interest in the community, CO_2 and CO reduction and N_2 reduction, have numerous possible products including the competing hydrogen evolution.¹¹⁻¹⁵ Thus, the next major frontier for computational electrocatalysis is to determine product selectivity and competing reaction pathways with high fidelity models.^{16,17}

In parallel, uncertainty quantification and propagation has emerged as an important approach that allows us in a systematic way to determine the fidelity of density functional

theory predictions.^{18–20} Building on the built-in error estimation capability in the Bayesian Error Estimation Functional with van der Waals (BEEF-vdW) exchange correlation (XC) functional, we have used this for optimal descriptor selection to predict electrocatalytic activity,²¹ quantify confidence in surface phase diagrams,^{22,23} and determine a variety of bulk properties.^{24,25} Most notably, in a previous study, we have defined a quantity called prediction efficiency, which provides a quantitative measure of the ability to distinguish the activity of materials and can be used to identify the optimal descriptor(s).²¹ However, the problem of determining product selectivity and the limiting step is a classification problem. Thus, it is important to quantify how robust the determined reaction product is to the choice of the exchange correlation functional.

In this work, we address the challenge of determining the optimal choice of descriptor(s) from the standpoint of maximizing the ability to classify product selectivity and the limiting elementary step(s). In order to do this, we define a quantity termed as classification efficiency, which is a measure of the ability to classify the outcome (for example reaction product, limiting the elementary step) using computations with finite accuracy. Based on this quantity, we can precisely determine the optimal descriptor(s) by maximizing the classification efficiency over the material range of interest. Specifically, we demonstrate this approach on the reactions of oxygen reduction and evolution and find that the free energy of the OOH* intermediate is the optimal descriptor for the former and that a two-descriptor model with the free energies of the OH* and O* intermediates is optimal for the latter. We believe that this approach will be extremely important for multi-electron electrochemical reactions such as CO₂ and N₂ reduction.

II. METHODS

A. Calculation details

All DFT calculations were performed using the projector augmented-wave (PAW) method²⁶ as implemented in the GPAW package²⁷ with the Bayesian Error Estimation Functional with van der Waals (BEEF-vdW) exchange correlation functional, which has built-in error estimation capabilities. For all adsorption free energy calculations, the two bottom layers of the unit cell were kept fixed and the top two layers with the adsorbates were allowed to relax with a force criterion of <0.05 eV/Å. A Fermi smearing of 0.01 eV was used, and all calculated energies were extrapolated to an electronic temperature of 0 K. Gas phase H₂O was used as the reference state for oxygen by assuming equilibrium with liquid water at 298 K and 0.035 bar,³ to avoid well-known errors within DFT in describing the energy of O₂. The effect of the electric field in the Helmholtz layer is not taken into account as this effect is negligible for adsorbates with small dipole moments perpendicular to the surface.²⁸

The BEEF-vdW functional is developed on the basis of Bayesian statistics, which defines the probability distribution

(P) denoted as $P(a|\theta, D) \sim \exp[-C(a)/\tau]$ where a represents model parameters of the model, θ , and training data set, D . $C(a)$ represents the cost function to avoid over-fitting, and τ denotes the cost “temperature.” Given a dataset, D , consisting of experimental sets of energetic and structural data describing bonding in chemical and condensed matter systems, a model perturbation, represented as δa , is associated with a probability that defines an ensemble of exchange correlation functionals.²⁹ The electron density derived from a self-consistent DFT calculation converged with the best-fit model parameters is used with the distribution of fitting parameters to generate an ensemble of energies non-self-consistently, which has shown to be representative of the error in the predictions of best-fit functional with respect to the experimental training data.^{24,25,29–31} The cost temperature (τ) is chosen such that the generated ensemble energies reproduce known experimental errors in the entire benchmark dataset, with no ensemble rescaling,³⁰ consistent with our prior studies.^{21,24,25,31}

In this work, the effect of solvation on the free energies of adsorbed intermediates is assumed to be negligible on the considered rutile (110) oxide surfaces owing to the hydrophobic nature of the oxide surfaces due to which a well-connected water network is typically not present and not in the registry with the underlying oxide surface.^{32,33} Although the effect of solvation based on the interaction of water molecules on metal surfaces has led to more accurate activity predictions,^{34–38} the effect of the water layer interaction and the solvation structure of water around oxygen intermediates are not established on rutile oxide surfaces. Tackling this is beyond the scope of the current work.

B. Bayesian error estimation framework and the ensemble-based approach

A systematic methodology to estimate the uncertainty in energetics computed through DFT calculations exists with the recent development of the Bayesian Ensemble Error Functional with van der Waals correlations (BEEF-vdW),²⁹ which is a semi-empirical exchange correlation (XC) functional including non-local contributions, developed based on training datasets including chemisorption on solid surfaces, molecular formation energies, molecular reaction barriers, molecular reaction energies, non-covalent interactions, and solid-state properties. The exchange correlation energy in the BEEF-vdW XC functional is expressed as the sum of the exchange energy under the generalized gradient approximation (GGA) expanded using Legendre polynomials, the local density approximation (LDA) and the PBE³⁹ correlation energies, and the non-local correlation energy from vdW-DF2,⁴⁰ which is represented as

$$E_{\text{xc}} = \sum_m a_m E_m^{\text{GGA-x}} + \alpha_c E^{\text{LDA-c}} (1 - \alpha_c) E^{\text{PBE-c}} + E^{\text{nl-c}}.$$

The parameters a_m and α_c are optimized to obtain the best fit with respect to the training datasets. The error estimation capability within the functional is enabled by

deriving an ensemble of energies non-self-consistently from an ensemble of exchange correlation functionals using the electron density from the self-consistent DFT calculation. The ensemble of exchange correlation functionals is generated using a probability distribution function (PDF) of the parameters, a_m and α_c , such that the standard deviation of the ensemble of energies computed self-consistently using BEEF-vdW reproduces the standard deviation for the training properties.

We obtain an ensemble of scaling relations [Figs. S1(a) and S1(b)] between the oxygen intermediates from the ensemble of exchange correlation functionals within the BEEF-vdW functional, which allows us to construct an ensemble of free energy diagrams for a given material descriptor value based on a descriptor choice. For the example of $4e^-$ reduction of O_2 to H_2O , the activity descriptor choice, G_d , which is typically the adsorption free energy of an oxygen intermediate, fixes one free energy level of the three variable free energy levels (ΔG_{OOH^*} , ΔG_{O^*} and ΔG_{OH^*}) of the FED at a given temperature and pressure. The ensemble of scaling relations leads to an ensemble of free energies for the other two levels, with a resulting ensemble of free energy diagrams. The limiting potential for reduction to H_2O corresponding to the n th member of the ensemble of FEDs is given by $U_L^n = \min(U_L^{1,n}, U_L^{2,n}, U_L^{3,n}, U_L^{4,n})$, where $U_L^{i,n} = |\Delta G_i^n|$, the free energy of the i th step of the reduction process by protons at 0 V vs. the reversible hydrogen electrode (RHE). This results in an ensemble of limiting potentials, where each member is associated with a unique activity determining step, corresponding to the ensemble of GGA-level exchange correlation functionals. A similar approach is employed to obtain the ensemble of limiting potentials from the associated potential determining elementary steps for the oxygen evolution reaction.

C. Quantifying confidence in the predicted reaction pathway

The predicted active reaction pathway or a set of active pathways for a given reaction, for example, oxygen reduction or evolution, varies with materials as a function of the chosen material descriptor (denoted as G_d) represented as $p_{pred}(G_d)$, which maps any given value of the chosen descriptor to the corresponding prediction of active reaction pathway(s) from the set of possible selectivity outcomes denoted by $\{0, 1, 2, \dots, i, \dots, n\}$, where i denotes the i th pathway or a simultaneous occurrence of more than one pathway. $i = 0$ indicates no active reaction pathway and $n = 2^k - 1 = \left[\sum_{i=1}^k \binom{n}{i} \right] - 1$, where k is the number of distinct pathways, which equals 2 for the case of oxygen reduction on metal surfaces. For both oxygen reduction and oxygen evolution, predominantly the $4e^-$ and $2e^-$ pathways occur, leading to $n = 3$ for these reactions with $i = 3$ denoting an equal limiting potential for both pathways.

We quantify the confidence in the predicted reaction mechanism(s) as a function of the descriptor D through a Bayesian error-estimation approach as discussed in Sec. II B.

The ensemble of functionals results in an ensemble of free energy diagrams and thereby an ensemble of active reaction pathways, allowing us to obtain a measure of the confidence in a predicted reaction pathway by quantifying the agreement between functionals. We use the c -value,^{22,24} which in this context can be defined as the fraction of the ensemble that predicts that a given pathway is active, and a generalized relation can be written as

$$c_{p_{pred}=i}(G_d) = \frac{1}{N_{ens}} \sum_{n=1}^{N_{ens}} \delta(p_{pred}^n(G_d) - i), \quad (1)$$

where n denotes the n th functional, N_{ens} is the total number of functionals in the ensemble, and $\delta(x)$ denotes the Kronecker delta function.

D. Quantifying confidence in the predicted potential determining step

The predicted potential determining elementary step for an identified reaction pathway, which is a function of the chosen material descriptor, G_d , represented as $PDS(G_d)$ for the potential determining step (PDS), maps any given value of the chosen descriptor to the corresponding potential determining step from the set of possible pathways denoted by $\{1, 2, \dots, i, \dots, n\}$, where i denotes the i th elementary step. Therefore, for the $4e^-$ pathways and $2e^-$ pathways, $n = 4$ and $n = 2$, respectively.

We quantify the confidence in the predicted potential determining step for a given reaction pathway as a function of the descriptor D using a similar approach to that discussed in Sec. II C. The ensemble of functionals results in an ensemble of free energy diagrams and thereby an ensemble of potential determining steps, allowing us to obtain a measure of the confidence in a predicted potential determining step by quantifying the agreement between functionals. We define a c -value here as the fraction of the ensemble that predicts that a given step is the potential determining step, which can be expressed as

$$c_{PDS=i}(G_d) = \frac{1}{N_{ens}} \sum_{n=1}^{N_{ens}} \delta(PDS^n(G_d) - i), \quad (2)$$

where n denotes the n th functional, $\delta(x)$ denotes the Kronecker delta function, and N_{ens} refers to the total number of functionals in the ensemble.

E. Classification efficiency based descriptor ranking

We note that the optimal descriptor choice for maximizing predictability with respect to one material classification, for example identifying the activity determining elementary step, could be different from that for a different material classification, for example identifying pathway selectivity. Therefore, pertaining to each context, we define a descriptor classification efficiency over a range of descriptor values (ΔG_d^{start} to ΔG_d^{end}) of interest, $\eta_{cls} \Big|_{\Delta G_d^{start}}^{\Delta G_d^{end}}$, as a measure of the agreement between GGA-level functionals with respect to the corresponding material classification objective.

Descriptors can be ranked based on the predictability of the potential determining step (PDS) using the $\eta_{\text{cls}}^{\text{PDS}}$ based on the highest c value, $c_{\text{MPDS}}(G_d, \sigma \rightarrow 0)$, over a range of descriptor values of interest, which is computed as

$$\eta_{\text{cls}}^{\text{PDS}} \Big|_{\Delta G_d^{\text{start}}^{\text{end}}} = \frac{\int_{\Delta G_d^{\text{start}}^{\text{end}}} c_{\text{MPDS}}(G_d, \sigma) dG_d}{\int_{\Delta G_d^{\text{start}}^{\text{end}}} c_{\text{MPDS}}(G_d, \sigma \rightarrow 0) dG_d}. \quad (3)$$

Similarly, descriptors can be ranked based on the predictability of pathway selectivity (active mechanism) using the $\eta_{\text{cls}}^{\text{sel}}$ based on the highest c value, $\max(c_{\text{sel}})(G_d, \sigma \rightarrow 0)$, over a range of descriptor values of interest, which is computed as

$$\eta_{\text{cls}}^{\text{sel}} \Big|_{\Delta G_d^{\text{start}}^{\text{end}}} = \frac{\int_{\Delta G_d^{\text{start}}^{\text{end}}} \max(c_{\text{sel}}(G_d, \sigma)) dG_d}{\int_{\Delta G_d^{\text{start}}^{\text{end}}} \max(c_{\text{sel}}(G_d, \sigma \rightarrow 0)) dG_d}. \quad (4)$$

For the two-descriptor model for the oxygen evolution reaction, we define the metric for predictability with respect to identifying the potential determining step (PDS) as

$$\eta_{\text{cls}}^{\text{PDS}} \Big|_{\Delta G_{d1}^{\text{start}}^{\text{end}}, \Delta G_{d2}^{\text{start}}^{\text{end}}} = \frac{\int_{\Delta G_{d1}^{\text{start}}^{\text{end}}} \int_{\Delta G_{d2}^{\text{start}}^{\text{end}}} c_{\text{MPDS}}(G_{d1}, G_{d2}, \sigma) dG_{d1} dG_{d2}}{\int_{\Delta G_{d1}^{\text{start}}^{\text{end}}} \int_{\Delta G_{d2}^{\text{start}}^{\text{end}}} c_{\text{MPDS}}(G_{d1}, G_{d2}, \sigma \rightarrow 0) dG_{d1} dG_{d2}}. \quad (5)$$

III. RESULTS

Our ensemble-based approach to robustly determining pathway selectivity and the activity determining elementary step(s) is demonstrated for the reactions of oxygen reduction and oxygen evolution.

A. Benchmarking of the adsorption free energy PDF

We perform a validation to address the issue of the physical meaningfulness of the ensemble of energies generated non-self-consistently within the BEEF-vdW XC functional. This is essential since a self-consistent method of estimating uncertainty (relaxing structure for every functional in the ensemble) is extremely computationally expensive. It is worth highlighting that there is sufficient evidence to suggest that the energy distribution generated using the non-self-consistent approach is a good representative sampling of the probability density function (PDF) of the computed free energy.^{21-25,30,31} In the context of this work, we show that energy distributions from this methodology bound the energy predictions by other GGA-level functionals: PBE, RPBE, and optPBE-vdW. Computed adsorption energy distributions of the oxygen intermediates calculated on the considered metal surfaces for oxygen reduction using the gas phase water and hydrogen reference scheme are shown in Figs. 1(b), 1(c), and 1(d). The error bars represent one standard

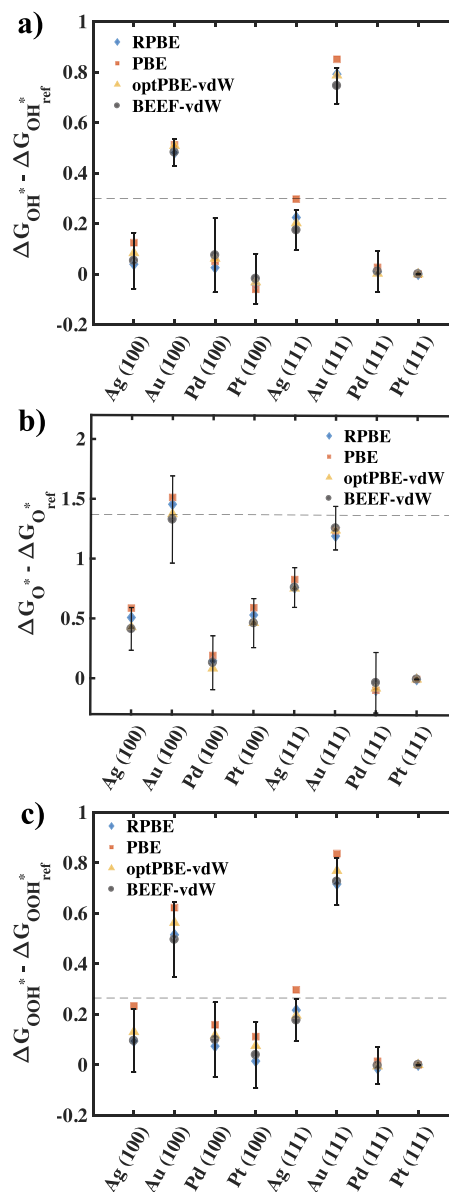


FIG. 1. Adsorption free energies of OH^* , O^* , and OOH^* on various transition metals as predicted by RPBE, PBE, optPBE-vdW, and BEEF-vdW XC functionals. The energies are referenced to the adsorption free energy of the corresponding intermediates on the Pt(111) surface. The error bars represent the standard deviation in the adsorption free energy as predicted by the ensemble of functionals generated using the BEEF-vdW XC. The dotted black line represents adsorption free energy of the intermediates on an “ideal” catalyst (peak of the activity volcano). We observe that the distribution emerging from the BEEF-vdW XC functional bounds the predictions by other functionals, indicating that this is a good representative probability density function for the predictions at the GGA-level of DFT.

deviation of the distribution computed from the BEEF-vdW XC functional, from which we demonstrate that the majority of the predicted energies lies within the one standard deviation bound estimated, which indicates that the obtained

distributions are a good representation of variations within the GGA-level of DFT. Similarly, Fig. 2 shows adsorption energy distributions of the three oxygen intermediates (O^* , OH^* , and OOH^* , respectively) calculated on the considered rutile oxides for oxygen evolution using the gas phase water and hydrogen reference scheme. We observe that a major

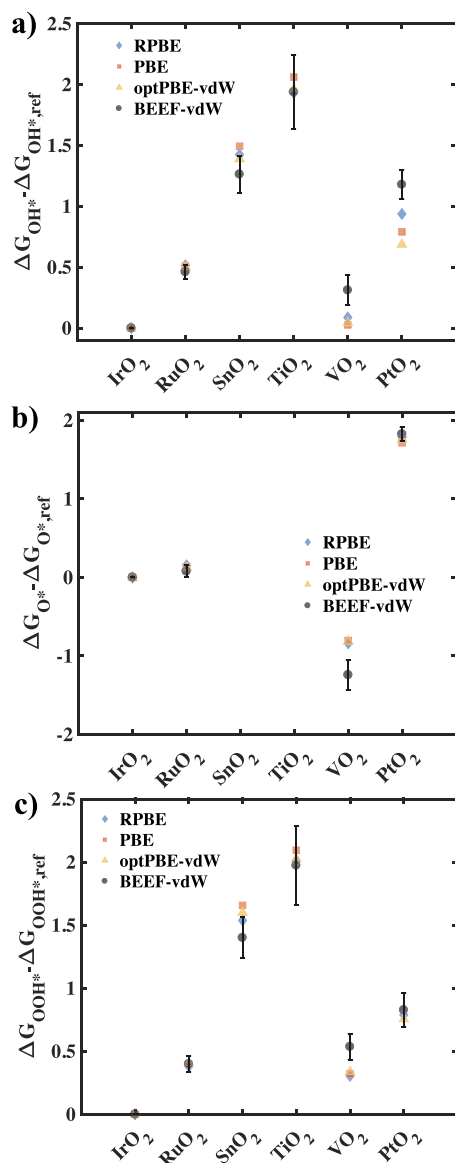


FIG. 2. Adsorption free energies of OH^* , O^* , and OOH^* on the (110) surface of various rutile oxide catalysts active for oxygen evolution as predicted by RPBE, PBE, optPBE-vdW, and BEEF-vdW XC functionals. The energies here are referenced to the adsorption free energy of various intermediates on IrO_2 . The error bars depict the standard deviation in the adsorption energy as predicted by the ensemble of functionals generated using the BEEF-vdW XC functional. This demonstrates that the distribution emerging from the BEEF-vdW XC functional is a reasonable representative probability density function for the predictions at the GGA-level of DFT for most metal oxides.

fraction of the energies predicted lies within the one standard deviation limits pertaining to the BEEF-vdW XC functional. It is worth noting that nearly all points lie within the two standard deviation limit since only $\approx 66\%$ of the data points lie within one standard deviation of a Gaussian distribution, which is a good approximation for the nature of the obtained energy distributions. This approach to quantitative error estimation in DFT is aimed at capturing the sensitivity of DFT-predicted properties to the choice of exchange-correlation approximation (defined by the model parameters a), which is an important source of uncertainty that has widely been applied to predictions of (electro)catalytic activity, mechanical properties of solids, magnetic ground states, stable surface species under electrochemical conditions, dominant reaction pathways, etc.^{21-25,30,31}

B. Oxygen reduction on metal surfaces

The mechanistic understanding of the oxygen reduction reaction (ORR) has predominantly been enabled by surface electrocatalysis on well-defined materials⁴¹⁻⁵⁰ through density functional theory calculations⁵¹⁻⁵⁷ in conjunction with surface analytical tools.^{47,50,58-61} Several descriptor-based computational screening approaches have been reported with different descriptor choices based on free energy scaling between the oxygen intermediates.^{31,62} Greeley *et al.* used the adsorption free energy of oxygen as the activity descriptor and demonstrated that Pt-based binary alloys have the potential to surpass the activity of Pt,⁶² while Ifan *et al.* used the free energy of OH^* intermediate as the descriptor to identify that Pt_5La exhibits activity of platinum.⁶³ In a recent study,²¹ we demonstrated a quantitative approach to choosing the right descriptor for maximizing the activity prediction efficiency given a threshold activity of interest. In this work, we use classification efficiency as a quantitative metric to identify the most appropriate descriptor choice(s) from the standpoint of maximizing the robustness of predictions of pathway selectivity and the activity determining elementary step.

A measure of the electrocatalytic activity for ORR is the limiting potential, which is determined by constructing the free energy diagram (FED) based on intermediates OOH^* , OH^* , and O^* by following the associative mechanism for the $4e^-$ and the $2e^-$ reduction pathways to H_2O and H_2O_2 , respectively.⁵¹ We transition from the simplified Sabatier volcano picture for ORR, where the potential determining step is assumed to be either $O_2 + H^+ + e^- \rightleftharpoons OOH^*$ or $OH^* + H^+ + e^- \rightleftharpoons H_2O$ (first step or the last, respectively) to determine the activity (limiting potential) from the limiting step of the FED. This transition to a higher fidelity model is particularly important for accurate activity determination of materials closer to the top of the volcano, which is where the primary focus of screening studies lies, due to the fact that the first and last elementary steps determine the activity for most materials that are very strong or weak binding. Therefore, given a descriptor choice,^{1,63,64} we utilize scaling relations⁶⁵ between these intermediates to construct the FED and thereby determine the limiting

potential. We consider several metal facets: Pt(111), Pt(100), Pt₃Ni(111), Au(111), Au(100), Ag(111), Ag(100), Pd(111), and Pd(100) to construct the scaling relations. Utilizing the Bayesian error estimation capabilities within the BEEF-vdW exchange correlation functional, we obtain an ensemble of scaling relations [Figs. S1(a) and S1(b)] between the oxygen intermediates. This allows us to construct an ensemble of free energy diagrams for a given descriptor choice and an associated descriptor value. We first discuss the case of the free energy of OH*, G_{OH^*} , as the descriptor, where the limiting potential for the $4e^-$ reduction to H₂O for the n th member of the ensemble of FEDs is given by $U_L^n = \min(U_L^{1,n}, U_L^{2,n}, U_L^{3,n}, U_L^{4,n})$, where $U_L^{i,n} = |\Delta G_i^n|$, the free energy of the i th step of the reduction process by protons. This results in an ensemble of limiting potentials, where each member is associated with a unique activity determining step, corresponding to the ensemble of GGA-level exchange correlation functionals within the BEEF-vdW family of functionals. A similar approach is employed to obtain the ensemble of limiting potentials from the associated potential determining elementary steps for the $2e^-$ oxygen reduction to H₂O₂.

We determine the most appropriate descriptor for maximizing prediction robustness of pathway selectivity based on the highest classification efficiency, η_{cls}^{sel} , η_{cls}^{sel} , $\eta_{cls}^{4e^-}$, and $\eta_{cls}^{2e^-}$ for a given descriptor are computed over a continuous descriptor range that encompasses the 1-standard-deviation ($1-\sigma$) limits of descriptor distributions of all considered metal surfaces. We find that the highest η_{cls}^{sel} occurs for the descriptor choice of ΔG_{OOH^*} . With confidence values (c-values) close to 1, which indicates a high degree of agreement between functionals at the GGA-level, we predict that the $4e^-$ reduction is thermodynamically favorable in the range $2.5 \lesssim \Delta G_{OOH^*} \lesssim 4.25$ eV and that both ($2e^-$ and $4e^-$) pathways are equally thermodynamically favorable in the range $\Delta G_{OOH^*} \gtrsim 4.25$. We rationalize the highest predictability corresponding to the descriptor ΔG_{OOH^*} based on the fact that OOH* is the only intermediate in the reduction to hydrogen peroxide and that the $2e^-$ activity can be computed without invoking scaling relations that have greater uncertainty. In these descriptor ranges, we identify based on $\eta_{cls}^{4e^-}$ and $\eta_{cls}^{2e^-}$ the optimal descriptors for robustly predicting the potential determining steps for the reduction to H₂O and H₂O₂, respectively. We find that ΔG_{OOH^*} as the descriptor leads to the highest η_{cls} for both the pathways. In the regime where the $4e^-$ reduction is predicted with high confidence, we predict that the OH* desorption step determines the potential with c-value ≈ 0.96 in the descriptor range $\Delta G_{OOH^*} \lesssim 3.8$ eV, beyond which we predict a smooth transition in the agreement between exchange correlation functionals to the OOH* adsorption step determining the potential. This trend is in agreement with prior literature since the OH* desorption step is known to be the limiting step for strong binding materials and the OOH* desorption step is known to be the limiting step for weak binding materials. In the regime where both the pathways are predicted to be equally favorable, we predict with high c-values (≈ 1) that the OOH* adsorption step is the potential determining step for both the $4e^-$ and $2e^-$ pathways.

We note that the optimal descriptor choice is a function of the materials of interest or the corresponding descriptor range. The range of interest for a given descriptor, ΔG_d ,

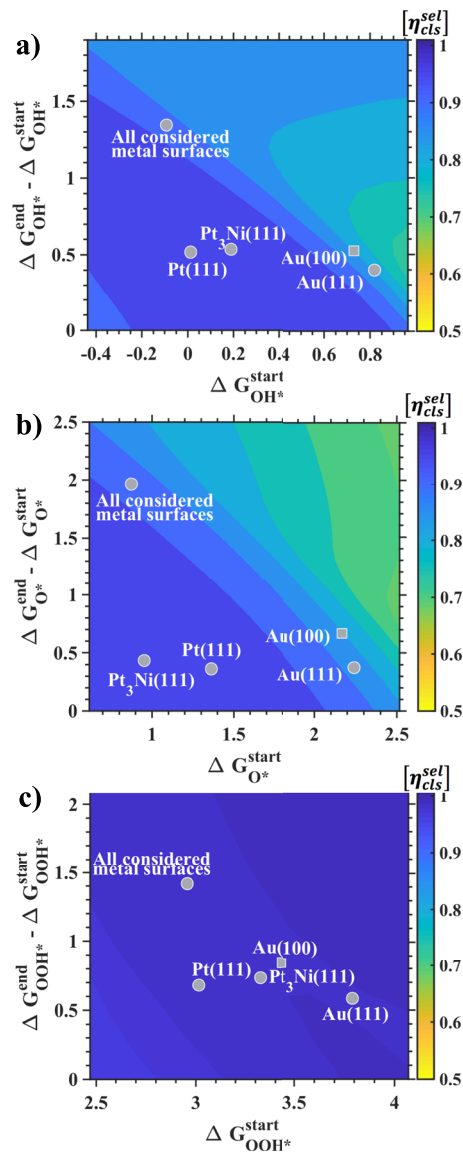


FIG. 3. Classification efficiency values quantifying the level of agreement between functionals as to the dominant pathway ($4e^-$ or $2e^-$), η_{cls}^{sel} , for the free energies of the three oxygen intermediates as potential descriptors. Since classification efficiency is defined over a range of descriptor values, the contour maps show η_{cls}^{sel} as a function of various ranges of interest uniquely represented by the start value and the width of the range, denoted as ΔG_d^{start} ΔG_d^{width} , respectively, where ΔG_d is the descriptor. We observe that over the range of descriptor values corresponding to all the considered metal surfaces, ΔG_{OOH^*} maximizes η_{cls}^{sel} . However, over descriptor ranges corresponding to the distribution of a specific metal facet, for example Pt(111) and Pt₃Ni(111), we find that multiple descriptors lead to equally high η_{cls}^{sel} values.

can be specified by the start value of the range, ΔG_d^{start} , and the width of the descriptor range, $\Delta G_d^{end} - \Delta G_d^{start}$. Figures 3 and 5 show the classification efficiency as a function of the descriptor range for the free energies of oxygen intermediates as descriptors. We observe from Fig. 3 that for the range of descriptor values corresponding to all the considered metal surfaces, the classification efficiency follows the trend $\eta_{cls}^{sel}(\Delta G_{OOH^*}) > \eta_{cls}^{sel}(\Delta G_{O^*}) \approx \eta_{cls}^{sel}(\Delta G_{OH^*})$, identifying that ΔG_{OOH^*} is the optimal descriptor for selectivity between the oxygen reduction to H_2O and H_2O_2 on the basis of agreement between functionals at the GGA-level level. The descriptor range of interest pertaining to each individual considered metal surface, computed as the continuous range between the corresponding 1σ limits from the DFT uncertainty is shown using gray dots. The classification efficiency value corresponding to each material represents the degree of agreement between functionals or the predictability with respect to pathway selectivity. It is worth noting that the classification efficiency value for a given material provides an *a priori* understanding of the DFT predictability for materials with very similar adsorption characteristics such as strained surfaces of the same material, which are likely to fall within the $1 - \sigma$ uncertainty limits. We rationalize our finding of the optimal descriptor (ΔG_{OOH^*}) for selectivity based on the fact that the intermediate OOH^* directly determines (no scaling relations involved) the $2e^-$ oxygen reduction activity and the fact that ΔG_{OH^*} and ΔG_{OOH^*} are both superior and near-optimal descriptors relative to ΔG_{O^*} as we demonstrate above (Table I).

The ability of the three descriptors to identify the limiting step for the corresponding pathway, determined based on the *c*-values shown in Fig. 4, can be compared using the classification efficiency metrics, $\eta_{cls}^{4e^-}$ and $\eta_{cls}^{2e^-}$, as shown in Fig. 5. For a given range of descriptor values of interest, the descriptor with the highest $\eta_{cls}^{4e^-}$ value indicates the highest degree of agreement between functionals as to the limiting step for the $4e^-$ oxygen reduction; the same applies to $\eta_{cls}^{2e^-}$ with respect to the $2e^-$ oxygen reduction. We observe that for the descriptor range corresponding to all the considered metal surfaces, the classification efficiency of the descriptors follows the trend $\eta_{cls}^{4e^-}(\Delta G_{OOH^*}) \approx \eta_{cls}^{4e^-}(\Delta G_{OH^*}) > \eta_{cls}^{4e^-}(\Delta G_{O^*})$, indicating that descriptors ΔG_{OOH^*} and ΔG_{OH^*} both lead to high identifiability of the limiting step. For smaller descriptor ranges of interest corresponding to specific materials such as Au(100) and Au(111), we find that higher predictability is achieved with ΔG_{OOH^*} relative to ΔG_{OH^*} as the descriptor, whereas Pt₃Ni(111) is an example of a material for which the

opposite trend holds, suggesting that ΔG_{OH^*} is a more appropriate descriptor for identifying the limiting step for the $4e^-$ oxygen reduction. We observe that for the $2e^-$ reduction to

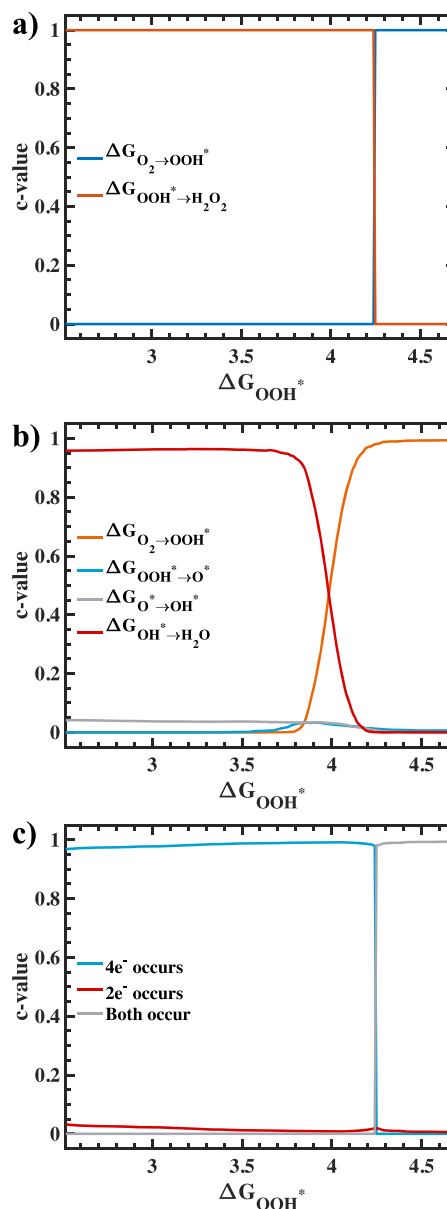


FIG. 4. Confidence values (*c* values) derived from the degree of agreement between functionals within the BEEF-vdW XC functional as to the dominant reaction pathway (c). *c* values associated with each step of the $2e^-$ and $4e^-$ pathways to H_2O_2 and H_2O indicating the robustness of predictions that a given step is the limiting (potential determining) step. For a given material, the prediction for the dominant reaction ($2e^-$ and $4e^-$) pathway can first be found based on (c), and for the identified pathway, the corresponding PDS can be observed from (a) and (b). In these figures, the confidence values are plotted on a material descriptor scale that maximizes the classification efficiency (η_{cls}) for the corresponding classification problem, which is computed to be ΔG_{OOH^*} for predictions of the dominant pathway and the corresponding potential determining step.

TABLE I. Comparison of η_{cls} for the oxygen reduction reaction on metal surfaces. ΔG_{OOH^*} as the descriptor leads to the highest classification efficiency for predicting both pathway selectivity and the associated limiting step(s).

Descriptor choice	η_{cls}^{sel}	$\eta_{cls}^{4e^-}$	$\eta_{cls}^{2e^-}$
ΔG_{OH^*}	0.893	0.917	0.912
ΔG_{O^*}	0.899	0.833	0.906
ΔG_{OOH^*}	0.985	0.936	1

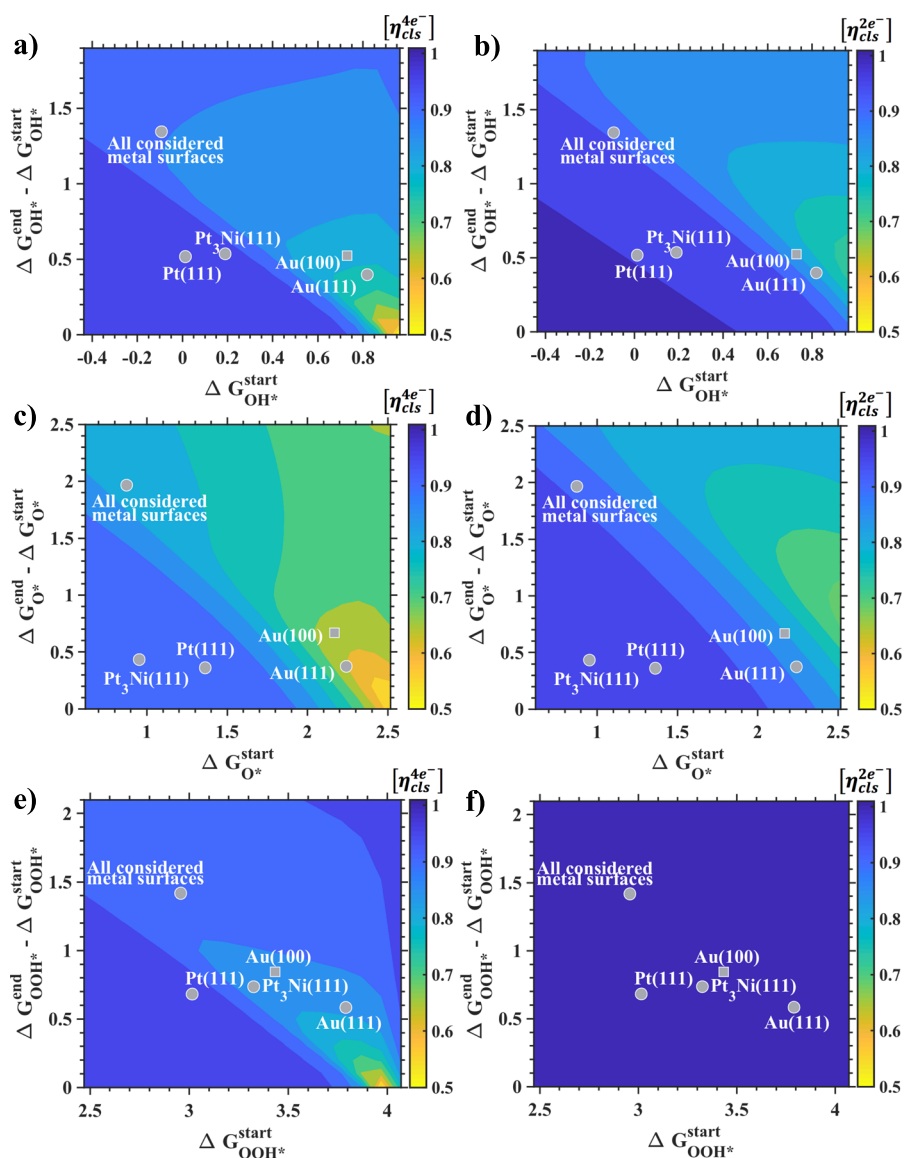


FIG. 5. c values indicating the robustness of predictions that the most thermodynamically favorable reaction pathway is the $4e^-$ reduction (left panel) or the $2e^-$ reduction (right panel), shown for the free energies of the oxygen intermediates as descriptors. Since classification efficiency is defined over a range of descriptor values, the contour maps show $\eta_{cls}^{4e^-}$ and $\eta_{cls}^{2e^-}$ as a function of various ranges of interest which can uniquely be represented by the start value and the width of the range. The points corresponding to individual metals are based on 1-standard-deviation limits from the distribution associated with the BEEF-vdW functional, which are also of interest when considering strained surfaces of the explored facets.

H_2O_2 , the universal optimal descriptor choice for identifying the limiting step is ΔG_{OOH^*} for all descriptor ranges of considered interest as can be seen from the relative $\eta_{cls}^{2e^-}$ values from Figs. 5(b), 5(d), and 5(f). We note that for this optimal descriptor choice, nearly all functionals are in agreement ($\eta_{cls}^{2e^-} \approx 1$) with respect to identifying the potential determining step for the $2e^-$ reduction to H_2O_2 . We rationalize the identified trends in predictability on the basis of the fact that the use of ΔG_{O^*} as the descriptor involves invoking two scaling relations in the construction of the free energy diagram, while ΔG_{OH^*} and ΔG_{OOH^*} use only one, leading to improved prediction efficiency. For the $2e^-$ reduction, the optimal descriptor choice of ΔG_{OOH^*} can be explained based on the fact that this intermediate is directly the tuning variable in controlling the activity for this reduction pathway.

C. Oxygen evolution on rutile oxides

We demonstrate the approach for oxygen evolution reaction, which is a crucial process for solar fuel generation and typically carried out under harsh oxidizing conditions.⁶⁶ The mechanistic understanding of the oxygen evolution reaction on metal oxide systems has been gained largely through experimental measurements.^{67,68} However, owing to the difficulty associated with preparing well-ordered single-crystalline oxides and the limited electrical conductivity, surface characterization and chemisorption energy measurements are challenging leading to limited insights developed using this approach.⁶⁹ Theoretical investigations have been limited by DFT accuracy in treating correlation energies in transition metal oxides,^{70,71} leading to

TABLE II. η_{cls} comparison for the oxygen evolution reaction on rutile oxide (110) surfaces. We observe that descriptor choices of $\{\Delta G_{\text{OH}^*}, \Delta G_{\text{O}^*}\}$ and $\{\Delta G_{\text{OOH}^*}, \Delta G_{\text{O}^*}\}$ lead to equally high $\eta_{\text{cls}}^{\text{sel}}$, indicating a high predictability of pathway selectivity, but the former choice is identified as the optimal descriptor since it leads to high predictability in terms of PDS classification for both the pathways.

Choice of descriptors	$\eta_{\text{cls}}^{\text{sel}}$	$\eta_{\text{cls}}^{4e^-}$	$\eta_{\text{cls}}^{2e^-}$
$\{\Delta G_{\text{OH}^*}, \Delta G_{\text{O}^*}\}$	0.97	0.95	1
$\{\Delta G_{\text{OOH}^*}, \Delta G_{\text{O}^*}\}$	0.97	0.94	0.95
$\{\Delta G_{\text{OOH}^*}, \Delta G_{\text{OH}^*}\}$	0.94	0.94	1

challenges in describing the surface electrochemistry. Martinez *et al.* showed that formation energies of rutile oxides can be described well at the GGA level within DFT using appropriate reference schemes.⁷² Later, the existence of scaling relations on rutile oxide and perovskite surfaces was shown by Man *et al.* and identified reactivity trends for oxygen evolution using the descriptor as the difference in the free energies of two oxygen intermediates, $\Delta G_{\text{O}^*} - \Delta G_{\text{OH}^*}$.¹ In a recent study, we formulated an approach to identifying the right descriptor(s) for maximizing the predictability of activity on the basis of quantitative metrics since multiple choices of descriptors

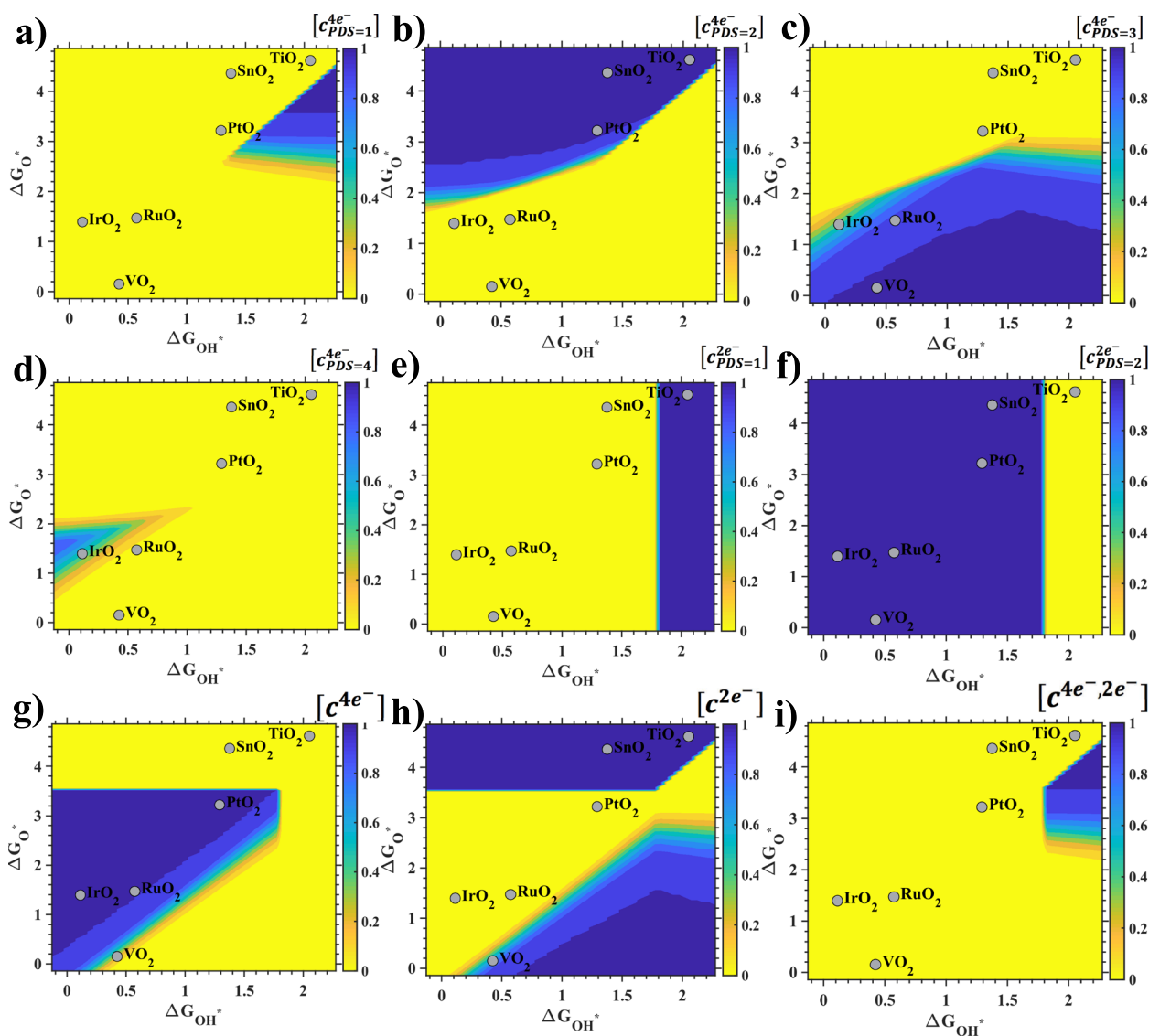


FIG. 6. c values representing the degree of agreement between functionals as to the pathway selectivity and the limiting step of the corresponding identified reaction pathway using the set of descriptors, $\{\Delta G_{\text{OH}^*}, \Delta G_{\text{O}^*}\}$, that maximize $\eta_{\text{cls}}^{\text{sel}}$, $\eta_{\text{cls}}^{4e^-}$, and $\eta_{\text{cls}}^{2e^-}$. (a)–(d) show the confidence values for the individual steps of the $4e^-$ oxidation pathway to O_2 , and (e) and (f) show the same for the $2e^-$ pathway to H_2O_2 . (g)–(i) show confidence values for the predictions of pathway selectivity toward the $4e^-$ pathway, the $2e^-$ pathway, and both, respectively, based on thermodynamic favorability.

have been explored without a common rationale.⁷³ In this work, on the basis of the classification efficiency, we present a quantitative approach to determining optimal descriptor(s) for identifying pathway selectivity and activity limiting steps.

We consider oxygen evolution on rutile oxide (110) surfaces of IrO₂, RuO₂, SnO₂, TiO₂, VO₂, and PtO₂ by assuming the associative mechanism.¹ We find that the scaling between the adsorption energies of OOH* and OH* has a slope close to 1 and the intercept is found to be 3.05.^{1,74} We construct the ensemble of free energy diagrams for the surfaces by employing a two-descriptor model similar to prior computational studies^{6,73} for higher predictability relative to a one-descriptor model. We explore all the combinations of 2-descriptor models involving the free energies of the three oxygen intermediates, ΔG_{OH^*} , ΔG_{O^*} , and ΔG_{OOH^*} , for the construction of free energy diagrams. We identify optimal descriptors for maximizing predictability of pathway selectivity using $\eta_{\text{cls}}^{\text{sel}}$ and that of limiting elementary step(s) using $\eta_{\text{cls}}^{\text{ne-}}$ for the corresponding pathway (n indicates n -step pathway) based on the ensemble approach outlined in Sec. II E. We compute $\eta_{\text{cls}}^{\text{sel}}$ and $\eta_{\text{cls}}^{\text{ne-}}$ for each two-descriptor model over the corresponding continuous ranges of descriptor values that encompass the 1-standard-deviation limits of the considered rutile oxide surfaces. We identify based on our analysis that for identifying pathway selectivity, descriptor combinations $\{\Delta G_{\text{OOH}^*}, \Delta G_{\text{O}^*}\}$ and $\{\Delta G_{\text{OH}^*}, \Delta G_{\text{O}^*}\}$ both lead to high (≈ 0.97) selectivity classification efficiency values (Table II) implying a high degree of agreement between functionals at the GGA level. However, it is worth highlighting that the descriptor combination $\{\Delta G_{\text{OH}^*}, \Delta G_{\text{O}^*}\}$ leads to higher predictability in terms of identifying the limiting steps corresponding to the $4e^-$ and $2e^-$ oxidation pathways. Therefore, we find that the optimal 2-descriptor model involves the free energies of intermediates ΔG_{OH^*} and ΔG_{O^*} on rutile oxide materials of interest. c -values corresponding to selectivity between oxidation pathways to H₂O₂ and O₂ and those pertaining to identifying the PDS for the respective pathways are shown in Fig. 6. We predict with high confidence (c -value ≈ 1) that materials PtO₂, IrO₂, and RuO₂ undergo the $4e^-$ oxidation pathway. We note that although RuO₂ lies close to low confidence values, all functionals suggest that the $4e^-$ pathway is the most thermodynamically favorable, indicating a high degree of agreement between the functionals. It is worth highlighting that such conclusions are uniquely possible through a Bayesian error estimation framework as employed in this study and represent a powerful aspect of such ensemble-based approaches. For these materials identified with the $4e^-$ oxidation pathway as the most favorable, we find that the oxidation step from OH* to O* is the limiting step for PtO₂, while the oxidation from O* to OOH* determines the potential for IrO₂. Similarly, we identify with high certainty (c -value ≈ 1) that TiO₂ and SnO₂ undergo the $2e^-$ oxidation pathway, for which our analysis suggests based on Figs. 6(e) and 6(f) that the activation of water as adsorbed OH* on the surfaces is the limiting step for SnO₂, whereas for TiO₂, the second step given by the desorption of OH* as H₂O₂ is the potential determining step.

IV. CONCLUSIONS

The developed quantitative framework based on the ensemble of energies derived from the Bayesian error estimation functional allows us to compute the confidence in the classification problem of pathway selectivity toward different reaction products and to identify the associated potential determining step for material candidates. The quantity defined in this work, referred to as classification efficiency, provides a basis for identifying optimal descriptor(s) for predicting selectivity toward different reaction products and the limiting step(s) for the corresponding pathway. For the first demonstrated example reaction of oxygen reduction, we show that ΔG_{OOH^*} is the optimal descriptor to classify materials between the $2e^-$ and $4e^-$ pathways for oxygen reduction. Similarly, for oxygen evolution, all 2-descriptor models were explored to identify that $\{\Delta G_{\text{OOH}^*}, \Delta G_{\text{O}^*}\}$ and $\{\Delta G_{\text{OH}^*}, \Delta G_{\text{O}^*}\}$ are both highly efficient at classifying between the $2e^-$ and $4e^-$ pathways for water oxidation. It is worth noting that although the descriptor PDFs in this work have been derived from the Bayesian error estimation framework within the BEEF-vdW XC functional, the presented quantitative methodology is applicable regardless of the origin of the descriptor distribution. The descriptor PDF could, for example, be obtained from machine learning models⁷⁵ that aim to reproduce experimental uncertainty associated with training datasets. The developed approach can directly be applied to other multi-electron electrochemical reactions such as CO₂ and N₂ reduction for improved mechanistic insights.

SUPPLEMENTARY MATERIAL

See [supplementary material](#) for additional information on calculation details and ranking of descriptors on the basis of classification efficiency metrics.

ACKNOWLEDGMENTS

D.K. and V.V. gratefully acknowledge funding support from the National Science Foundation under Award No. CBET-1554273. V.V. and V.S. acknowledge support from the Scott Institute for Energy Innovation at Carnegie Mellon University.

REFERENCES

- 1 I. C. Man, H.-Y. Su, F. Calle-Vallejo, H. A. Hansen, J. I. Martínez, N. G. Inoglu, J. Kitchin, T. F. Jaramillo, J. K. Nørskov, and J. Rossmeisl, *ChemCatChem* **3**, 1159 (2011).
- 2 V. Viswanathan, H. Hansen, J. Rossmeisl, and J. K. Nørskov, *ACS Catal.* **2**, 1654 (2012).
- 3 J. K. Nørskov, T. Bligaard, A. Logadottir, J. Kitchin, J. G. Chen, S. Pandelov, and U. Stimming, *J. Electrochem. Soc.* **152**, J23 (2005).
- 4 J. Greeley and J. K. Nørskov, *J. Phys. Chem. C* **113**, 4932 (2009).
- 5 N. B. Halck, V. Petrykin, P. Krtil, and J. Rossmeisl, *Phys. Chem. Chem. Phys.* **16**, 13682 (2014).
- 6 S. Siahrostami, G.-L. Li, V. Viswanathan, and J. K. Nørskov, *J. Phys. Chem. Lett.* **8**, 1157 (2017).
- 7 V. Viswanathan, H. A. Hansen, J. Rossmeisl, and J. K. Nørskov, *J. Phys. Chem. Lett.* **3**, 2948 (2012).

- ⁸H. A. Hansen, V. Viswanathan, and J. K. Nørskov, *J. Phys. Chem. C* **118**, 6706 (2014).
- ⁹V. Viswanathan, H. A. Hansen, and J. K. Nørskov, *J. Phys. Chem. Lett.* **6**, 4224 (2015).
- ¹⁰K. S. Exner, I. Sohrabnejad-Eskan, J. Anton, T. Jacob, and H. Over, *Chem-ElectroChem* **4**, 2902 (2017).
- ¹¹H. A. Hansen, J. B. Varley, A. A. Peterson, and J. K. Nørskov, *J. Phys. Chem. Lett.* **4**, 388 (2013).
- ¹²J. Hussain, H. Jónsson, and E. Skúlason, *ACS Catal.* **8**, 5240 (2018).
- ¹³E. Skulason, T. Bligaard, S. Gudmundsdóttir, F. Studt, J. Rossmeisl, F. Abild-Pedersen, T. Vegge, H. Jónsson, and J. K. Nørskov, *Phys. Chem. Chem. Phys.* **14**, 1235 (2012).
- ¹⁴S. Hanselman, M. T. Koper, and F. Calle-Vallejo, *ACS Energy Lett.* **3**, 1062 (2018).
- ¹⁵A. J. Göttle and M. T. Koper, *Chem. Sci.* **8**, 458 (2017).
- ¹⁶K. S. Exner, I. Sohrabnejad-Eskan, and H. Over, *ACS Catal.* **8**, 1864 (2018).
- ¹⁷Z. W. Seh, J. Kibsgaard, C. F. Dickens, I. Chorkendorff, J. K. Nørskov, and T. F. Jaramillo, *Science* **355**, eaad4998 (2017).
- ¹⁸J. J. Mortensen, K. Kaasbjerg, S. L. Frederiksen, J. K. Nørskov, J. P. Sethna, and K. W. Jacobsen, *Phys. Rev. Lett.* **95**, 216401 (2005).
- ¹⁹V. Petzold, T. Bligaard, and K. Jacobsen, *Top. Catal.* **55**, 402 (2012).
- ²⁰J. Wellendorff, K. T. Lundgaard, K. W. Jacobsen, and T. Bligaard, *J. Chem. Phys.* **140**, 144107 (2014).
- ²¹D. Krishnamurthy, V. Sumaria, and V. Viswanathan, *J. Phys. Chem. Lett.* **9**, 588 (2018).
- ²²V. Sumaria, D. Krishnamurthy, and V. Viswanathan, *ACS Catal.* **8**, 9034 (2018).
- ²³O. Vinogradova, D. Krishnamurthy, V. Pande, and V. Viswanathan, *Langmuir* **34**, 12259 (2018).
- ²⁴G. Houchins and V. Viswanathan, *Phys. Rev. B* **96**, 134426 (2017).
- ²⁵Z. Ahmad and V. Viswanathan, *Phys. Rev. B* **94**, 064105 (2016).
- ²⁶J. J. Mortensen, L. B. Hansen, and K. W. Jacobsen, *Phys. Rev. B* **71**, 035109 (2005).
- ²⁷J. E. Enkovaara, C. Rostgaard, J. J. Mortensen, J. Chen, M. Dulak, L. Ferrighi, J. Gavnholt, C. Glinsvad, V. Haikola, and H. Hansen, *J. Phys.: Condens. Matter* **22**, 253202 (2010).
- ²⁸G. Karlberg, J. Rossmeisl, and J. K. Nørskov, *Phys. Chem. Chem. Phys.* **9**, 5158 (2007).
- ²⁹J. Wellendorff, K. T. Lundgaard, A. Møgelhøj, V. Petzold, D. D. Landis, J. K. Nørskov, T. Bligaard, and K. W. Jacobsen, *Phys. Rev. B* **85**, 235149 (2012).
- ³⁰A. J. Medford, J. Wellendorff, A. Vojvodic, F. Studt, F. Abild-Pedersen, K. W. Jacobsen, T. Bligaard, and J. K. Nørskov, *Science* **345**, 197 (2014).
- ³¹S. Deshpande, J. R. Kitchin, and V. Viswanathan, *ACS Catal.* **6**, 5251 (2016).
- ³²Z. Zeng and J. Greeley, *Nano Energy* **29**, 369 (2016).
- ³³J. Rossmeisl, Z.-W. Qu, H. Zhu, G.-J. Kroes, and J. K. Nørskov, *J. Electroanal. Chem.* **607**, 83 (2007).
- ³⁴J. A. Gauthier, C. F. Dickens, L. D. Chen, A. D. Doyle, and J. K. Nørskov, *J. Phys. Chem. C* **121**, 11455 (2017).
- ³⁵Z.-D. He, S. Hanselman, Y.-X. Chen, M. T. M. Koper, and F. Calle-Vallejo, *J. Phys. Chem. Lett.* **8**, 2243 (2017).
- ³⁶F. Calle-Vallejo, A. Krabbe, and J. M. Garcia-Lastra, *Chem. Sci.* **8**, 124 (2017).
- ³⁷P. A. Thiel and T. E. Madey, *Surf. Sci. Rep.* **7**, 211 (1987).
- ³⁸D. T. Limmer, A. P. Willard, P. Madden, and D. Chandler, *Proc. Natl. Acad. Sci. U. S. A.* **110**, 4200 (2013).
- ³⁹J. P. Perdew, K. Burke, and M. Ernzerhof, *Phys. Rev. Lett.* **77**, 3865 (1996).
- ⁴⁰K. Lee, É. D. Murray, L. Kong, B. I. Lundqvist, and D. C. Langreth, *Phys. Rev. B* **82**, 081101 (2010).
- ⁴¹N. Marković and P. N. Ross, *Surf. Sci. Rep.* **45**, 117 (2002).
- ⁴²S. Mukerjee, S. Srinivasan, M. P. Soriaga, and J. McBreen, *J. Electrochem. Soc.* **142**, 1409 (1995).
- ⁴³N. M. Markovic, H. A. Gasteiger, and P. N. Ross, Jr., *J. Phys. Chem.* **99**, 3411 (1995).
- ⁴⁴J. Zhang, M. B. Vukmirovic, Y. Xu, M. Mavrikakis, and R. R. Adzic, *Angew. Chem., Int. Ed.* **44**, 2132 (2005).
- ⁴⁵W. P. Zhou, X. Yang, M. B. Vukmirovic, B. E. Koel, J. Jiao, G. Peng, M. Mavrikakis, and R. R. Adzic, *J. Am. Chem. Soc.* **131**, 12755 (2009).
- ⁴⁶A. Kuzume, E. Herrero, and J. M. Feliu, *J. Electroanal. Chem.* **599**, 333 (2007).
- ⁴⁷M. Wakisaka, H. Suzuki, S. Mitsui, H. Uchida, and M. Watanabe, *Langmuir* **25**, 1897 (2009).
- ⁴⁸M. Wakisaka, Y. Udagawa, H. Suzuki, H. Uchida, and M. Watanabe, *Energy Environ. Sci.* **4**, 1662 (2011).
- ⁴⁹S. Kondo, M. Nakamura, N. Maki, and N. Hoshi, *J. Phys. Chem. C* **113**, 12625 (2009).
- ⁵⁰I. E. Stephens, A. S. Bondarenko, F. J. Perez-Alonso, F. Calle-Vallejo, L. Bech, T. P. Johansson, A. K. Jepsen, R. Frydendal, B. P. Knudsen, and J. Rossmeisl, *J. Am. Chem. Soc.* **133**, 5485 (2011).
- ⁵¹J. K. Nørskov, J. Rossmeisl, A. Logadottir, L. Lindqvist, J. R. Kitchin, T. Bligaard, and H. Jónsson, *J. Phys. Chem. B* **108**, 17886 (2004).
- ⁵²A. B. Anderson, *Electrochim. Acta* **47**, 3759 (2002).
- ⁵³V. Viswanathan, H. A. Hansen, J. Rossmeisl, T. F. Jaramillo, H. Pitsch, and J. K. Nørskov, *J. Phys. Chem. C* **116**, 4698 (2012).
- ⁵⁴Y. Gohda, S. Schnur, and A. Groß, *Faraday Discuss.* **140**, 233 (2009).
- ⁵⁵M. J. Janik, C. D. Taylor, and M. Neurock, *J. Electrochem. Soc.* **156**, B126 (2009).
- ⁵⁶A. B. Anderson, J. Uddin, and R. Jinnouchi, *J. Phys. Chem. C* **114**, 14946 (2010).
- ⁵⁷R. Jinnouchi, T. Hatanaka, Y. Morimoto, and M. Osawa, *Phys. Chem. Chem. Phys.* **14**, 3208 (2012).
- ⁵⁸A. Damjanovic, M. Genshaw, and J. Bockris, *J. Electrochem. Soc.* **114**, 1107 (1967).
- ⁵⁹J. L. Fernández and A. J. Bard, *Anal. Chem.* **75**, 2967 (2003).
- ⁶⁰H. Hoster, B. Richter, and R. Behm, *J. Phys. Chem. B* **108**, 14780 (2004).
- ⁶¹V. R. Stamenkovic, B. Fowler, B. S. Mun, G. Wang, P. N. Ross, C. A. Lucas, and N. M. Markovic, *Science* **315**, 493 (2007).
- ⁶²J. Greeley, I. Stephens, A. Bondarenko, T. P. Johansson, H. A. Hansen, T. Jaramillo, J. Rossmeisl, I. Chorkendorff, and J. K. Nørskov, *Nat. Chem.* **1**, 552 (2009).
- ⁶³I. E. Stephens, A. S. Bondarenko, U. Grønberg, J. Rossmeisl, and I. Chorkendorff, *Energy Environ. Sci.* **5**, 6744 (2012).
- ⁶⁴F. Calle-Vallejo and M. T. Koper, *Electrochim. Acta* **84**, 3 (2012).
- ⁶⁵F. Abild-Pedersen, J. Greeley, F. Studt, J. Rossmeisl, T. Munter, P. G. Moses, E. Skulason, T. Bligaard, and J. K. Nørskov, *Phys. Rev. Lett.* **99**, 016105 (2007).
- ⁶⁶N. S. Lewis and D. G. Nocera, *Proc. Natl. Acad. Sci. U. S. A.* **103**, 15729 (2006).
- ⁶⁷S. Trasatti, *Electrochim. Acta* **29**, 1503 (1984).
- ⁶⁸S. Trasatti, *J. Electroanal. Chem. Interfacial Electrochem.* **111**, 125 (1980).
- ⁶⁹C. T. Campbell and J. R. Sellers, *Chem. Rev.* **113**, 4106 (2013).
- ⁷⁰A. J. Cohen, P. Mori-Sánchez, and W. Yang, *Science* **321**, 792 (2008).
- ⁷¹L. Wang, T. Maxisch, and G. Ceder, *Phys. Rev. B* **73**, 195107 (2006).
- ⁷²J. I. Martinez, H. A. Hansen, J. Rossmeisl, and J. K. Nørskov, *Phys. Rev. B* **79**, 045120 (2009).
- ⁷³L. C. Seitz, C. F. Dickens, K. Nishio, Y. Hikita, J. Montoya, A. Doyle, C. Kirk, A. Vojvodic, H. Y. Hwang, J. K. Nørskov, and T. F. Jaramillo, *Science* **353**, 1011 (2016).
- ⁷⁴V. Viswanathan and H. A. Hansen, *Top. Catal.* **57**, 215 (2014).
- ⁷⁵J. Ling, M. Hutchinson, E. Antono, S. Paradiso, and B. Meredig, *Integr. Mater. Manuf. Innovation* **6**, 207 (2017).